Proposal to PAC38

Polarized Electrons for Polarized Positrons:
A proof–of–principle experiment

Hari Areti[1], Maud Baylac[2], Germain Bosson[2], Alexandre Camsonne[1], Larry Cardman[1], Olivier Dadoun[3], Jonathan Dumas[1,2], Erica Fanchini[2], Tony Forest[5], Arne Freyberger[1], Serkan Golge, Joseph Grames[1], Paul Guèye[4], Yujong Kim[1,5], Jean-François Muraz[2], Marc Marton[2], Matt Poelker[1], Jean-Sébastien Réal[2], Riad Suleiman[1], Alessandro Variola[3], Eric Voutier[2]

[1] *Thomas Jefferson National Accelerator Facility*
12000 Jefferson Avenue
Newport News, Virginia 23606, USA

[2] *Laboratoire de Physique Subatomique et de Cosmologie*
IN2P3/CNRS, Université Joseph Fourier, INP
53 rue des Martyrs
38026 Grenoble cedex, France

[3] *Laboratoire de l'Accélérateur Linéaire*
IN2P3/CNRS, Université Paris-Sud
Bât. 200 - BP 34
91898 Orsay cedex, France

[4] *Physics Department*
Hampton University
Hampton, VA 23668, USA

[5] *Department of Physics and Idaho Accelerater Center*
Idaho State University
Pocatello, ID 83209, USA

Abstract

Contact persons: grames@jlab.org, voutier@lpsc.in2p3.fr

Table of contents

1 Introduction

Symmetry properties in physics, either verified or violated, are the basis of a quantum theory and fundamental tools of experimental investigations. For instance: the CPT symmetry is considered as a basic and mandatory property of any physics law; within the standard model, the violation of the electroweak symmetry is associated to massive gauge bosons via the Higgs mechanism [1]; also, it is the spontaneous breaking of the chiral symmetry which confers to pions their very singular role in nuclear physics. On the experimental side, the violation of the parity symmetry in polarized electron scattering became over the past decade a privilegied tool for the investigation of the strange content of the nucleon [2–4] and develops today towards tests of the standard model [5]. As part of these fundamental experimental tools, the comparison between polarized electron and polarized positron scatterings takes advantage of the inteference with the single photon exchange to isolate peculiar features of physics [6].

The power of polarization observables for the study of the most intimate structure of matter has been demonstrated in many experiments at SLAC, CERN, DESY, RHIC and JLab. Nowadays, polarization is the finest probe of the nuclear structure and it became an essential part of the next accelerator generation. The development of a powerfull and low cost polarized positrons source is one of the technological challenges of these new machines.

An efficient scheme for positron production, widely used in particle accelerators, relies on the creation of electron-positron pairs from high energy photons. A significant aspect of the process is the dependence on the polarization, in particular, the circular polarization of the photon transfers to the longitudinal polarization of the positron [7]. This is the basic concept of operation of polarized positron sources developped for the International Linear Collider (ILC). The circularly polarized photons are here produced either from the Compton back-scattering of a laser light off high energy electrons [8] or from the synchrotron radiation of very high energy electrons travelling through a helical undulator [9]. The present experiment proposed to investigate an alternative scheme based on the polarized bremsstralhung process [10].

Similarly to pair creation, the bremsstralhung process is a polarization sensitive mechanism. This property has been widely used at un-polarized electron accelerators to produce linearly polarized photon beams. In addition to the intrinsic linear polarization, the photons have a circular component when the incoming electron beam is polarized, such that the bremsstrahlung of polarized electrons most generally lead to elliptically polarized photons [7,11]. This concept is routinely used to obtain a linearly or a circularly polarized photon beam at the Jefferson Laboratory (JLab) Hall B [12] at several GeV beam energy.

The production of polarized positrons from polarized bremsstrahlung [13,14] was explored in the ILC context but not pursued because of limited performances. Most recent advances in high-polarization (85 %) and high-current (1 mA) electron sources [15] overcome these technical limits and offer a greater

potential for a compact, low energy driver for a polarized positron source [16]. However, the basic operational concept that is the transfer of the longitudinal polarization of electrons to positrons via polarized bremsstrahlung and subsequent polarized pair-creation was never experimentally investigated. It is the goal of the present experiment to demonstrate and quantify this concept by measuring the energy distribution of the positron yield and polarization obtained from a low energy (6.3 MeV) highly polarized electron beam in the 2-5 MeV energy range.

This document is organized as followed. The next section presents the motivations of the proposed experiment, particularly the importance of this measurement for the understanding of the polarization transfert physics. The benefit of a polarized positron beam for the investigation of the partonic structure of the nucleon is also discussed, together with the opportunities at very low energies (< 200 keV) for solid state physics studies. The following sections review the experimental apparatus and principle of operation. The proposed experimental methodology and beam requirements are described in the last section.

2 Motivations

Polarized and unpolarized positron beams are complementary and essential tools for the understanding of numerous physics phenomena ranging from high energy physics to solid state physics (see ref. [6] for an overview). The PEPPo experiment (Polarized Electrons for Polarized Positrons) is the first step of a longer term program aiming at the development of an intense polarized posiron source to serve, at high energy in the next accelerator generation (JLab, SuperB, ELIC...), and at very low energy in the development of a new tool to study the structure of condensed matter.

2.1 Polarization transfert in bremsstralhung and pair creation processes

2.1.1 Relavistic approach

As the essential mechanism for the production of high energy photons, the bremsstrahlung process is a text-book reaction widely investigated theoretically and experimentally. Polarization observables were first addressed by H. Olsen and L. Maximon [7] (hereafter referred to as OM) within the Born approximation for relativistic and small angle particles, including effects of the nuclear field screening and corrections to the Born approximation. These are still today the reference calculations implemented in the GEANT4 simulation package [17,18]. The circular polarization transfer is essentially universal, the highest circular polarization being obtained at the highest photon energy (fig. 1 left). A similar behaviour is observed at low energies but with the additionnal feature of an unphysical region close to the end point of the spectra (fig. 1 right). This appears in the calculations as a consequence of the well-known tip problem: due to too large Coulomb corrections for heavy nuclei, the

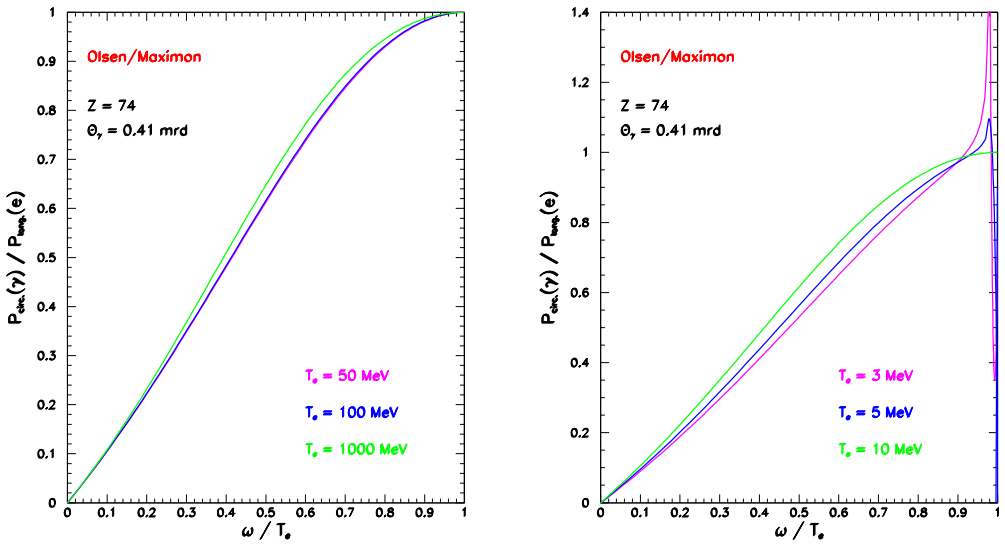

Figure 1. Longitudinal to circular polarization transfer for the bremsstrahlung process according to OM prescription at high (left) and low (right) initial electron kinetic energy.

OM unpolarized differential cross section passes zero and becomes negative. This translates into a singularity for the polarization transfer in the tip region.

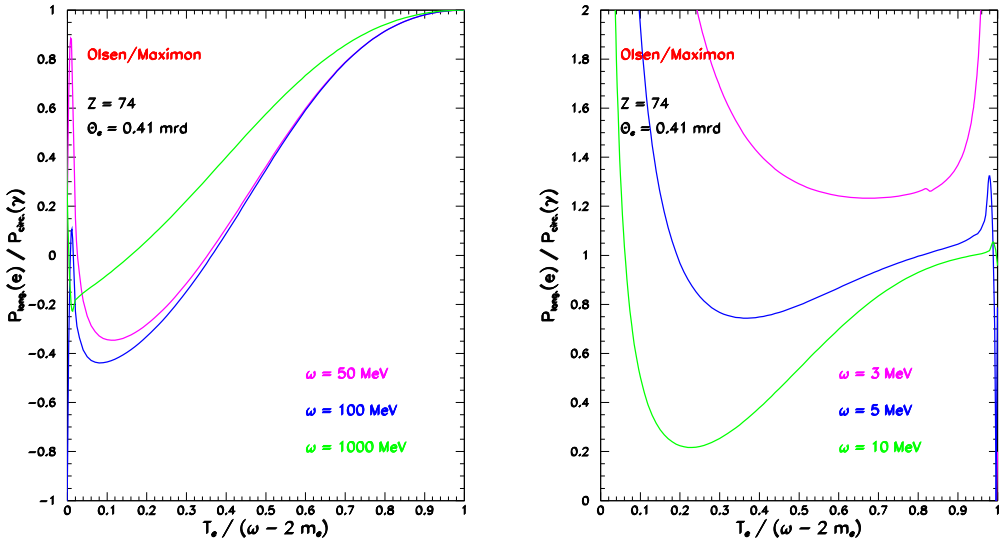

Figure 2. Circular to longitudinal polarization transfer for the pair creation process according to OM prescription at high (left) and low (right) initial photon energy.

As a reciprocal process of the bremsstrahlung reaction, pair production is described by the same matrix elements so that the relations for experimental observables can be derived from the bremsstralhung expressions following elementary substitutions [7]. The polarization transfer from circular photons to longitudinal positrons appears to be more sensitivite to the initial photon energy than in the bremsstrahlung case. These calculations clearly show some singular behaviour even at high energy (fig. 2 left) i.e. in a region where OM approximations are expected to be valid. It is even more stricking at low en-

ergy where these relations yield unphysical results (fig. 2 right) over a large part if not all of the kinematic phase space. As surprising it may be, polarization phenomena in the pair creation process are not understood within OM prescription.

2.1.2 Electron mass effects

These phenomena were recently revisited by E. Kuraev et al. [19] (hereafter referred to as KBST) taking advantage of the most modern techniques to reformulate in the infinite momentum frame the matrix elements of the bremmstrahlung and pair creation reactions. Polarization observables are rederived within this framework in the Born approximation, neglecting Coulomb corrections but considering screening effects and specifically taking into account the effects of finite electron mass.

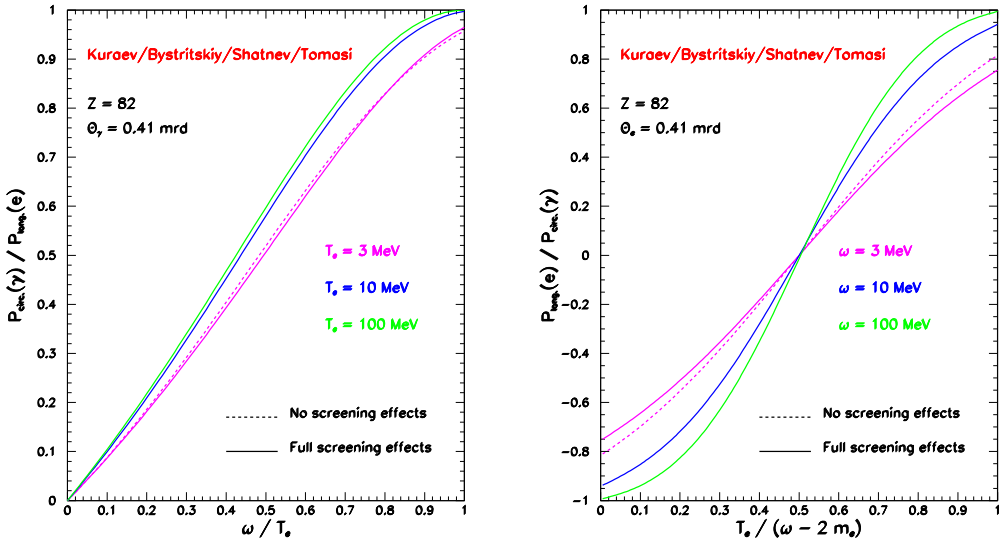

Figure 3. Longitudinal polarization transfer in the bremsstrahlung process (left) and circular polarization transfer in the pair creation process according to the KBST prescription at different initial energies.

The KBST calculations dont exhibit any of the singular features of OM calculations and the comparison between the two extreme screening situations (none and full) show moderate and mastered effects (fig. 3). The description of the bremsstrahlung process is numerically very close to OM and is free of end-point effects. Furthermore, within the KBST approach, the polarization transfer for the pair creation process possesses the very remarkable feature of a kinematical symmetry. It is indeed quite natural to expect such a symmetry in a process where only two particles with same mass and spin are produced. The differences between OM and KBST calculations for this process (fig. 4) are the largest at small energy and significantly persist at high energy as a consequence of the observed kinematical symmetry.

The main result of this new approach is the consistent description of both the bremmsstrahlung and pair creation processes with no constraint on the initial beam energy. This is a direct consequence of the finitie mass of the

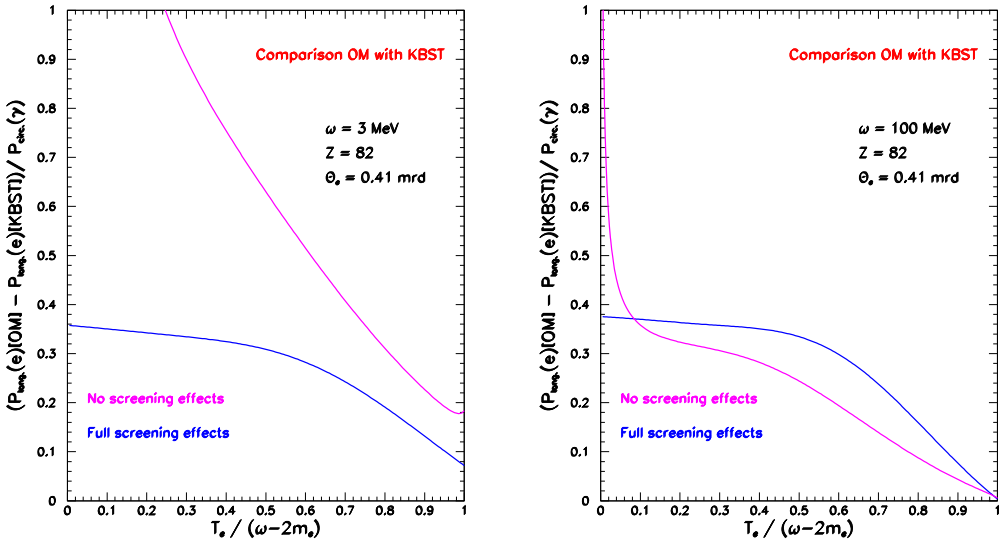

Figure 4. Difference between OM and KBST prescriptions for the circular polarization transfer in the pair creation process at low (left) and high (right) initial photon energy.

electron and is further supported by noticing that OM calculations become unphysical in kinematical regions where the electron mass is physically important: when the initial electron gives all of its kinetic energy to the photon (bremmstrahlung); when one particle of the e^+e^- pair is produced at rest and also at low photon energy (pair creation). Even if bremsstrahlung and pair creation are reciprocal processes, some of the OM approximations valid for the bremsstrahlung reaction cannot be exported to the pair creation process.

By measuring the polarization transfert from longitudinal electrons to longitudinal positrons at low energy and off a thin target, the PEPPo experiment will provide the necessary data to understand polarization phenomena in the pair creation process.

2.2 Nucleon structure studies

In the context of the hadronic physics program worked out at JLab, the comparison between electron and positron scatterings is not only an additionnal source of information but also a mandatory step for the extraction of the physics quantities of interest [6]. Particularly, the accurate investigation of the partonic structure of nucleons and nuclei ask for both polarized electrons and polarized positrons.

2.2.1 Generalized parton distributions

It is only recently that a comprehensive picture of the nucleon structure started to develop, within the framework of the generalized parton distributions (GPDs) [20,21]. These distributions parametrize the partonic structure of the nucleon in terms of correlations between quarks, anti-quarks and glu-

ons, and therefore contain information about the dynamics of this system. The power of this framework for the problem of the nucleon structure is certainly within the Mellin moments of the GPDs [22] which provide a natural link between microscopic and macroscopic properties of the nucleon.

GPDs are universal non-perturbative objects entering the description of hard scattering processes and correspond to the amplitude for removing a parton carrying some longitudinal momentum fraction and restoring it with a different ones (fig. 5). In this process, the nucleon receives a four-momentum transfer whose transverse component is Fourier conjugate to the transverse position of partons. Consequently, GPDs can be interpreted as a distribution in the transverse plane of partons carrying a certain longitudinal momentum [23–26], constituting a femto-tomography of the nucleon.
At the leading twist, the partonic structure of the nucleon [22,27] is described by four quark helicity conserving and chiral even GPDs ($H^q, \widetilde{H}^q, E^q, \widetilde{E}^q$) and four quark helicity flipping and chiral odd GPDs ($H^q_T, \widetilde{H}^q_T, E^q_T, \widetilde{E}^q_T$), together with eight similar gluon GPDs. In the forward limit ($t \to 0, \xi \to 0$), the optical theorem links the H GPDs to the usual density, helicity, and tranversity distributions measured in deep inelastic scattering (DIS). However, the E GPDs, which involve a flip of the nucleon spin, do not have any DIS equivalent and then constitute a new piece of information about the nucleon structure. The first Mellin moments relate chiral even GPDs to form factors, as E^q with the Pauli electromagnetic form factor and the second Mellin moments relate GPDs to the nucleon dynamics, particularly the total angular momentum carried by the partons, following Ji's sum rule [28]. Similar relations have been proposed which relate chiral odd GPDs to the transverse spin-flavor dipole moment and the correlation between quark spin and angular momentum in an unpolarized nucleon [29].

2.2.2 Deeply virtual Compton scattering

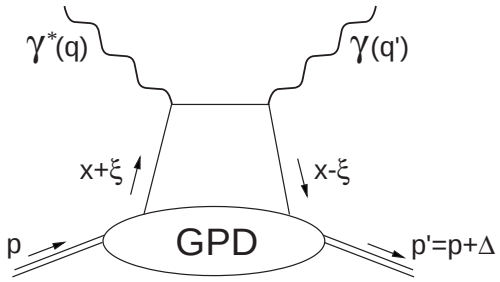

Figure 5. Lowest order (QCD) amplitude for the virtual Compton process.

GPDs can be accessed in the Bjorken regime [30,31] of deep exclusive processes, that is when the resolution power of the probe is large enough to resolve partons and when the momentum transfer to the nucleon is small enough to insure the separation of perturbative and non-perturbative scales. Pioneer measurements at HERMES [32] and CLAS [33], and recent JLab experiments [34–36] have established the relevance of the DVCS process for this studies.

DVCS, corresponding to the absorption of a virtual photon by a quark followed

quasi-instantaneously by the emission of a real photon, is the simplest reaction to access GPDs. In the Bjorken regime, the leading contribution to the reaction amplitude is represented by the so-called handbag diagram (fig. 5) which figures the convolution of a known $\gamma^* q \rightarrow \gamma q$ hard scattering kernel with an unknown soft matrix element describing the partonic structure of the nucleon parametrized by GPDs. Consequently, GPDs (E^f) enter the reaction cross section through a Compton form factor $\mathcal{E}$ which involves an integral over the intermediate quark propagator

$$\mathcal{E} = \sum_f e_f^2 \, \mathcal{P} \int_{-1}^{+1} dx \left(\frac{1}{\xi - x} - \frac{1}{\xi + x} \right) E^f(Q^2, x, \xi, t) + i\pi \sum_f e_f^2 \left[E^f(Q^2, \xi, \xi, t) - E^f(Q^2, -\xi, \xi, t) \right] , \quad (1)$$

leading to a complex DVCS amplitude which real and imaginary parts are the quantities of interest to be extracted from experimental data.

In addition to the DVCS amplitude, the cross section for electroproduction of photons gets contributions from the Bethe-Heitler (BH) process where the real photon is emitted by the initial or final lepton, leading to [37]

$$\sigma(ep \rightarrow ep\gamma) = \sigma_{BH} + \sigma_{DVCS} + P_l \, \widetilde{\sigma}_{DVCS} + e_l \, \sigma_{INT} + P_l e_l \, \widetilde{\sigma}_{INT} + S \left[P_l \, \Delta\sigma_{BH} + P_l \, \Delta\sigma_{DVCS} + \Delta\widetilde{\sigma}_{DVCS} + P_l e_l \, \Delta\sigma_{INT} + e_l \, \Delta\widetilde{\sigma}_{INT} \right] \quad (2)$$

where the $[\Delta]\sigma(\widetilde{\sigma})$'s are even(odd) function of the out-of-plane angle between the leptonic and hadronic planes; S is the longitudinal or transverse polarization of the target; P_l and e_l are the lepton polarization and charge, respectively. Though undistinguishable from DVCS, the BH cross section is known and exactly calculable from the electromagnetic form factors. The pure DVCS and interference contributions contain the information of interest, particularly $[\Delta]\sigma_{INT}(\widetilde{\sigma}_{INT})$ is proportionnal to the real(imaginary) part of the DVCS amplitude. The knowledge of the full set of the eight unknown amplitudes participating to the reaction cross section is required in order to separate in a model independent way the different GPDs [38,39]. Considering for simplicity the case of an unpolarized target, the observables measured with a (un)polarized electron beam are

$$\sigma^0(e^-) = \sigma_{BH} + \sigma_{DVCS} - \sigma_{INT} \quad (3)$$

$$\sigma^+(e^-) - \sigma^-(e^-) = 2P_l \, \widetilde{\sigma}_{DVCS} - 2P_l \, \widetilde{\sigma}_{INT} \quad (4)$$

where the upper index denotes the polarization state of the beam. Separating further the DVCS and INT contributions requires additionnal measurements at different beam energies within a Rosenbluth like procedure [40] which is known to be limited in the case of elastic electron scattering. The availability of a polarized positron beam allows the measurement of the additional observables

$$\sigma^0(e^+) - \sigma^0(e^-) = 2\,\sigma_{INT} \tag{5}$$

$$\left[\sigma^+(e^+) - \sigma^+(e^-)\right] - \left[\sigma^-(e^+) - \sigma^-(e^-)\right] = 4P_l\,\widetilde{\sigma}_{INT} \tag{6}$$

which correspond to a unique determination of the real and imaginary parts of the interference amplitude, free from any additional contributions.

In conclusion, the determination of the eight unkown contributions to the cross section for electroproduction of photons and the subsequent extraction of the nucleon GPDs require the measurement of eight independent observables that can be uniquely achieved combining polarized electrons and polarized positrons data.

2.3 Solid state structure studies

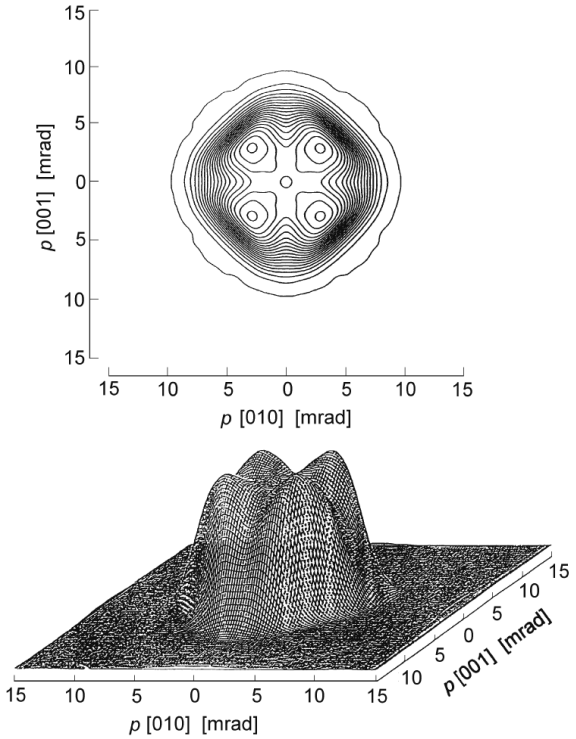

Figure 6. Two-dimensional angular correlation of annihilation radiation in gallium arsenide exhibiting no positron trapping in defects [42].

Positron Annihilation Spectroscopy (PAS) is a well-know technique for the investigation of the structure of materials [6], and particularly develops for the study of defects and vacancies in semi-conductors [41]. It relies on the annihilation of very low energy positrons with atomic electrons of the material and the subsequent detection of one or the pair of the generated photons. The decay time of this process is directly related to the electron density at the annihilation site. Furthermore, the motion of atomic electrons induce a Doppler broadening of the 511 keV γ-rays and a distortion of the back-to-back angular correlation. Consequently, the measurement of the energy distribution, or the angular correlation between annihilation γ-rays allow to characterize

the material via the determination of the momentum distribution of atomic electrons (fig. 6).

This powerfull technique, known as 2D-ACAR, is however limited by the intensity of the available positron sources usually obtained from radioactive sources. The generation of positrons from small energy electrons is expected to deliver 100 times higher positron flux [43]. Together with polarization capabilities, such accelerator based thermalized positron sources would be a breakthrough for PAS studies.

3 PEPPo apparatus

3.1 Principle of the PEPPo experiment

3.2 PEPPo electron beamline - Region 0

The Region 0 of the PEPPo experiments is a part of an existing CEBAF injector beamline between a viewer (ITV0L01) and a dipole (MBV0L021) as shown in Fig. 7. By tuning strength of existing three quadrupoles (MQJ0L01, MQJ0L02, and MQJ0L02A) in the Region 0, we can adjust the transverse beam size or beam diameter at the electron-positron converting target, which is the first target at the Region 1. To match the electron beam optics along the PEPPo beamline, the transverse electron beam emittance and twiss parameters (α, β, γ) will be measured by using a well-known quadrupole scanning method. To perform the quadrupole scanning method, a quadrupole (MQJ0L01) and the second viewer (ITV0L02) in the Region 0 will be used. Electron beam energy and energy spread will also be measured with the dipole magnet and a viewer (ITV2D00) in the -30 deg spectrometer beamline as shown in Fig. 7. These measured twiss parameters, transverse beam emittance, energy, and energy spread will be used to update a design optics of electron beams along the PEPPo beamline. For the PEPPo experiments, a new branching beamline (+25 degree beamline) will be added to the dipole, and the dipole will be rotated to make the pole face angles of the dipole magnet perpendicular to the beam trajectory of the 0 degree CEBAF injector beamline shown in Fig 8. Since the maximum value of multiplication of the magnetic field and the effective length of the dipole magnet is about 14833 G-cm for a maximum power supply current of 3.5 A, its maximum bending angle is about 33.8 degree for 8 MeV electron beam. Therefore, by adjusting current of the magnet power supply, the dipole can supply electron beams to four branching beamlines (-30 degree spectrometer, -12.5 degree mott polarimeter, 0 degree CEBAF injector, and +25 degree PEPPo) freely as shown in Figs. 8 and 9.

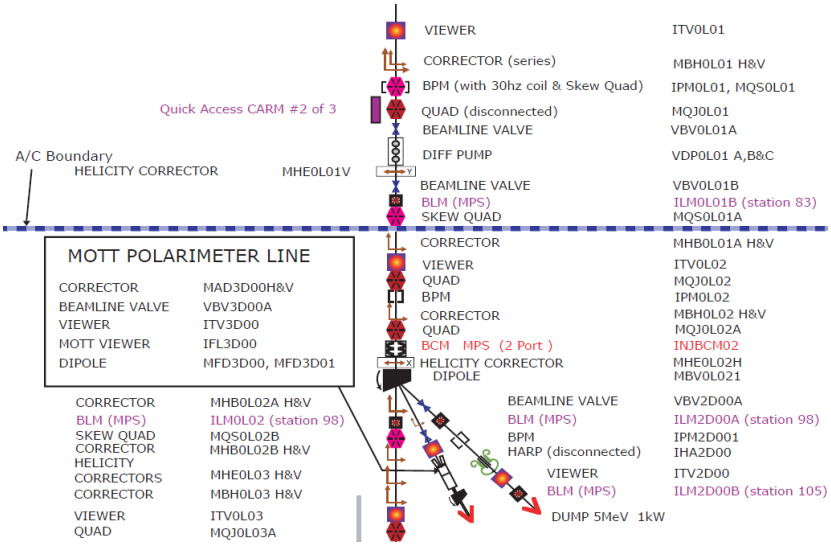

Figure 7. Layout of the Region 0 of the PEPPo beamline.

3.3 PEPPo electron beamline - Region 1

The Region 1 of the PEPPo experiments is a new electron beamline from the MBV0L021 dipole to the electron-positron converting first target, which is located at S = 62.96“ as shown in Fig. 8. Since the natural horizontal dispersion at the first target is about 0.7 m, and expected relative rms energy

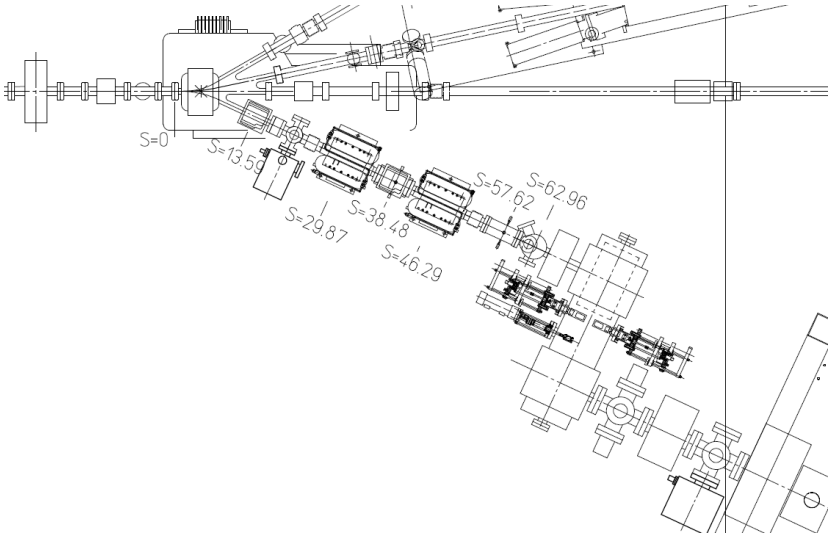

Figure 8. Layout of the Region 1 of the PEPPo beamline. Here the beamline is rotated by -90 degree from the layout in Fig. 7.

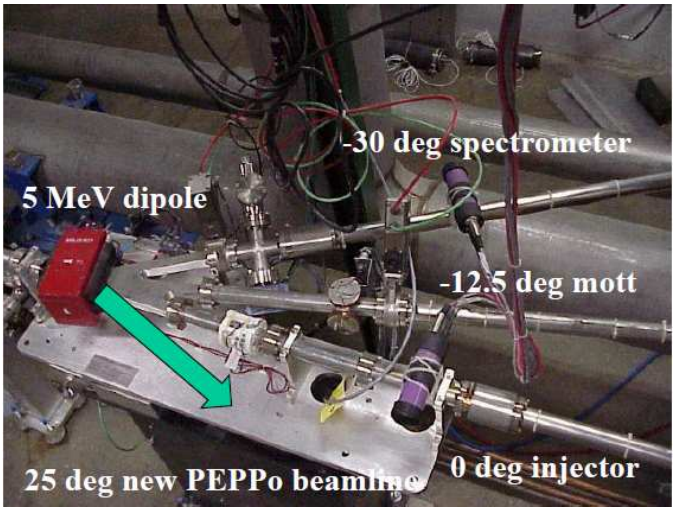

Figure 9. Three existing beamlines and a new PEPPo beamline of a dipole (MBV0L021).

spread of electron beam is about 0.1%, the horizontal beam size is much bigger than the vertical beam size if the horizontal dispersion function is not reduced properly. To reduce the horizontal dispersion function at the first target, two new quadrupoles will be installed at S = 29.87" and S = 46.29" as shown in Fig. 8. By optimizing two new quadrupoles in the Region 1, we can reduce the horizontal dispersion function at the first target, and we can also make a round beam shape at the first target as shown in Figs. 10 and 11.

By optimizing three quadrupoles in the Region 0 and two quadrupoles in Region 1 together, the beam diameter at the first target can be adjustable from 1.0 mm to 6 mm as shown in Fig. 11.

To detect and to compensate electron beam positions and to compensate the angle of beam trajectory in the Region 1, there are two beam position monitors at S = 38.48" and S = 57.62" and two horizontal and vertical steering magnet set at S = 13.59" and S = 38.48" as shown in Fig. 8. In addition to the beam position monitors, there are two viewers to measure beam energy, energy spread, beam size, beam trajectory, and the horizontal dispersion function in the Region 1.

For a kinetic energy of 6.3 MeV, electron beam parameters and machine parameters are summarized in Table 1.

3.4 PEPPo positron line

3.5 Compton transmission polarimeter

The measurement of positron polarization is made by first transferring the polarization to photons using a reconversion target, and then using a photon-transmission polarimeter. The layout of the positron polarimeter is shown in Fig. 13. Experimental apparatus has been loaned from E166 SLAC experiment

[44]. The photons that emerge from the reconversion target (0.5 rad. len. of tungsten) are incident on an 7.5 cm long (and 5 cm diameter) magnetized iron absorber. The photons that are transmitted through the absorber are detected in a CsI array of 9 crystals for which we measured between 3 and 4% of energy resolution for 0.662 MeV photons. Crystals are 28 cm long and 6 cm side.

At saturation, the overall longitudinal polarization of the iron target is 8.19%. Saturation is obtained using a solenoid magnet (see figure 12) over most of the cylindrical core. Averaged polarization value of the iron target were taken to be 0.069±0.002 [44]. The same procedure will be follow to extract averaged iron polarization. The magnetic field of the iron will be measured with several pickup coils surrounding the core of the magnet. The induced-voltage signal due to a change of the magnetic flux through the pickup coil will be measured with a Precision Digital Integrator PDI upon field reversal. The external Field map will also be measured to know the fringed field and to constraint the Opera-3D calculation. The expected polarization error is of the same order of magnetude that the one obtained for E166 (≃1%).

Photons transmitted by the iron target will be detected in CsI(Tl) crystal which measure the total energy. 9 crystals arranged in a 3x3 array are stacked in a brass chamber with 6mm wall thickness and a entrance window of 2mm thickness. The box is light tight and a continuous small flow of Nitrogen will evacuate the humidity and the heat. Each crystal is wrapped with two layers of white Tyvek paper to increase the scintillation light collection, and with a

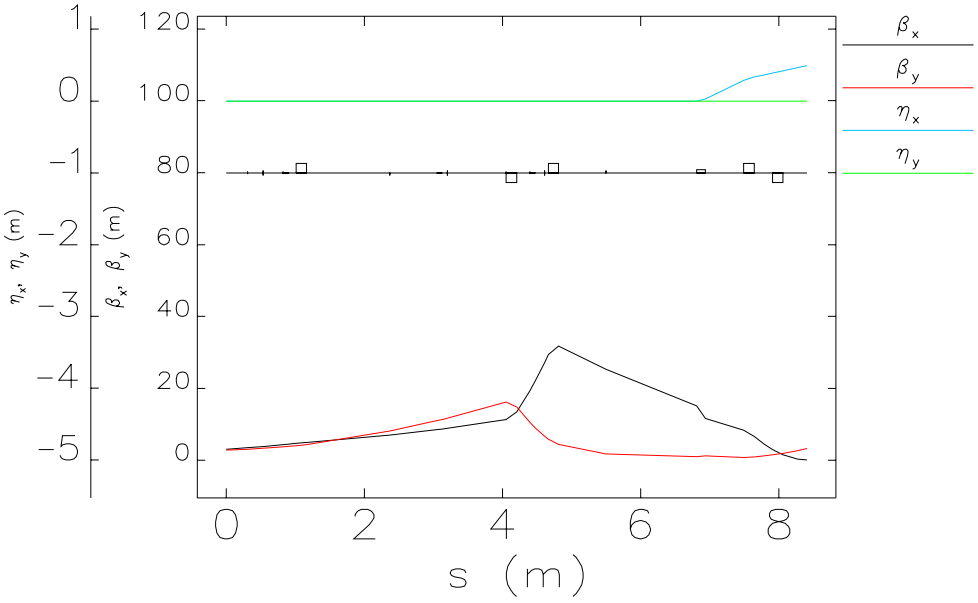

Figure 10. Electron beam optics along the PEPPo Region 0 and 1 to obtain a beam diameter of 3 mm at the first target. Here the beamline starts from 0.3 m upstream from the first viewer (ITV0L01) in the Region 0, and three quadrupoles in Region 0 are located at s ≃ 1.2 m, 4.2 m, and 4.8 m. The MBV0L021 dipole is located at s ≃ 6.9 m, and two new quadrupoles are located at s ≃ 7.6 m and 8.1 m. The first target is located at the end of the beamline, s ≃ 8.4 m.

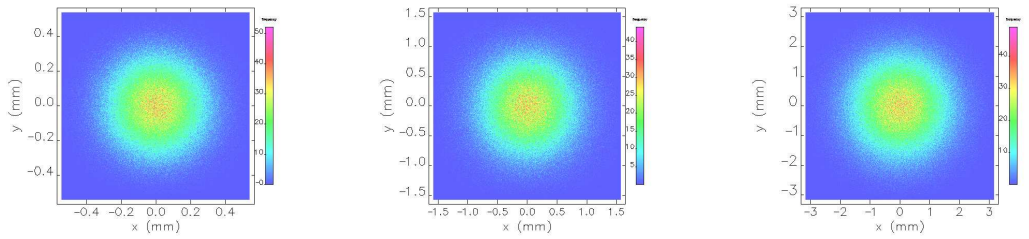

Figure 11. Transverse electron beam profiles at the first target for a beam diameter of 1 mm (left), 3 mm (center), and 6 mm (right).

Table 1
Beam and machine parameters in the Region 0 and Region 1.

Parameter	Unit	Value
electron kinetic energy	MeV	6.3
relative rms energy spread	%	0.1
rms bunch length	mm	0.3
single bunch charge	fC	20
average electron beam current	μA	10
electron beam operational frequency	MHz	499
initial horizontal alpha-function $\alpha_{x,0}$	·	-0.566
initial vertical alpha-function $\alpha_{y,0}$	·	-0.397
initial horizontal beta-function $\beta_{x,0}$	m	3.076
initial vertical beta-function $\beta_{y,0}$	m	2.798
maximum gradient of quadrupoles	T/m	10
mechanical length of quadrupole	m	0.15
final horizontal beta-function β_x	m	0.098
final vertical beta-function β_y	m	3.299
final horizontal dispersion η_x	m	0.492
rms beam size at the first target	mm	0.5
diameter of electron beam at the 1st target	mm	3
shape of transverse beam profile	·	Gaussian
shape of longitudinal beam profile	·	Gaussian

copper foil (30μm) to prevent cross-talk. Energy resolution of the crystal has been measured using a Cs137 source which emit 0.662 MeV photons.

Each crystal is coupled to photomultiplier (hamamatsu R6236) via a 3 mm thick optical silicon rubber. R6236 is a 8 dynode stages square photomulti-

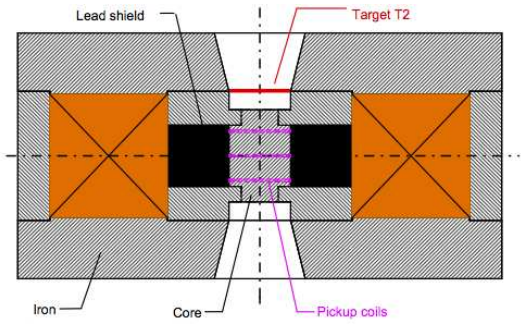

Figure 12. E166 positron analyzer magnet

plier. Mechanical size is 6 cm x 6 cm equivalent to the crystal size, and the photocathode Area Size is 5.4 cm X 5.4 cm. The PMts are readout using a house made socket which include a amplifier (X108). With typical high voltage ranging from 1050 V to 1400 V depending on the PMTs (maximum for these PMTs are 1500 V), we cover a wide range of photon energy ranging from 0.1 MeV to 5 Mev . output signal (50 Ohm) range from -40 mV to 1.9 V which is suitable for the FADC input.

A set of 5 scintillator paddles will be used to trig cosmic muons passing through the calorimeter. A coincidence of 2 scintillators above and 3 scintillators below the calorimeter will allow to measured the cosmic at minimum ionization and will give a absolute calibration of the 9 crystals in the same time. Energy loss of a minimum ionizing muon particle is 40 MeV for a crystals. In that case, amplifier of the socket has to be off, this done automatically by powering off upstairs the ± 12 V energizing the amplifier. Then the output amplitude of the cosmic will be around 140 mV and will go to a leading edge discriminator. The cosmic trigger will be done using a CAEN V895 discriminator using the MAjority logic which will be fired by 2 paddles over 5. The output of discriminator will then be sent to a tdc for offline selection. A rates of 1Hz was obtained during the test and several hours of counting is necessary. This calibration configuration can be used anytime when there is no beam without going into the tunnel.

A set of optical fibers coupled to the crystals will allow us to monitor the relative change in gain during operation for offline correction and time to time high voltage correction. 1 Hz or less LED trigger is done using a set of pulser and divider. The LED is fired by a negative pulse with an amplitude adjusted between 0 and -3 V.

Figure 13 shows a drawing of the existing calorimeter and table of the positron polarimeter. The calorimeter is space by 0.5 cm from the analyzer magnet, the brass box will be surrounded by some lead block to minimize background and to stop particles not coming from the analyzer target. The supporting plate of the magnet, the polarimeter and the shielding, can be move 20 cm forwards to insert some beam diagnostics.

4 PEPPo operation

4.1 Measurement principle

The differential cross section for the Compton scattering of circularly polarized photons (P_γ) off a polarized electron target (P_t) can be written

$$\frac{d^2\sigma}{d\theta d\phi} = \frac{d^2\sigma^0}{d\theta d\phi}\left[1 + P_\gamma P_t A_C(\theta)\right] \tag{7}$$

where $d^2\sigma^0/d\theta d\phi$ is the unpolarized Compton cross section

$$\frac{d^2\sigma^0}{d\theta d\phi} = \frac{1}{2}\left(r_0 \frac{\omega}{\omega_0}\right)^2 \left[\frac{\omega_0}{\omega} + \frac{\omega}{\omega_0} - \sin^2(\theta)\right] \sin(\theta)\,, \tag{8}$$

and

$$A_C(\theta) = \left[\frac{\omega_0}{\omega} - \frac{\omega}{\omega_0}\right] \cos(\theta) \Big/ \left[\frac{\omega_0}{\omega} + \frac{\omega}{\omega_0} - \sin^2(\theta)\right] \tag{9}$$

is the analyzing power of the Compton process, both quantities depending on the scattered photon energy (ω) and angle (θ), and the incoming photon energy (ω_0).

Compton transmission polarimetry takes advantage of the sensivity of the Compton process to the absorption of circularly polarized photons in a polarized target. This method, which involves a single detection device matching the size of the incoming beam, is intrinsically easy to implement and has been recently used successfully in experiments similar to the present one [**?**,44]. Considering the simple case of a monochromatic parallel photon beam scattering off a polarized electron target with length L, the transmission efficiency characterizing the probability that a photon exits the target may be written

$$\varepsilon_T = \exp\left[-(\mu_0 + P_\gamma P_t \mu_1)L\right] \tag{10}$$

which assumes the loss of any photon interacting in the target and the dominance of the Compton process; μ_0 and μ_1 are the unpolarized and polarized Compton absorption coefficients

$$\mu_0 = \rho_e \int d\theta d\phi \frac{d^2\sigma^0}{d\theta d\phi} \qquad \mu_1 = \rho_e \int d\theta d\phi \frac{d^2\sigma^0}{d\theta d\phi} A_C(\theta) \tag{11}$$

with ρ_e the electron density of the target.

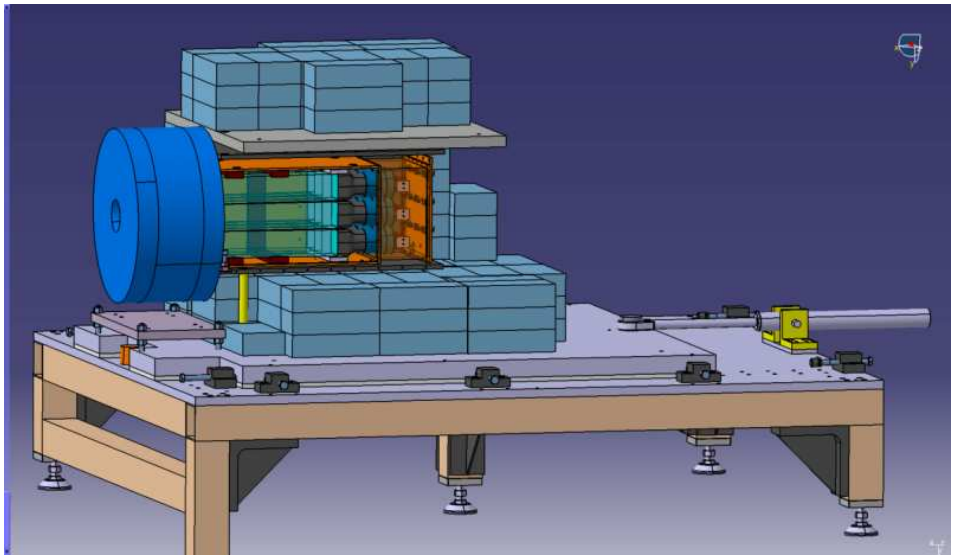

Figure 13. PEPPO positron polarimeter setup

The measurement of the circular polarization of the photon beam is obtained from the number of transmitted photons for opposite polarized target orientations. The corresponding asymmetry writes

$$A_T = \frac{N^+ - N^-}{N^+ + N^-} = \tanh(-P_\gamma P_t \mu_1 L) \tag{12}$$

from which the photon circular polarization is inferred according to

$$P_\gamma = -A_T / P_t \mu_1 L \,. \tag{13}$$

The associated statistical uncertainty writes

$$\delta P_\gamma = \left[2 N_\gamma \, P_t^2 \, \mu_1^2 L^2 \exp\left(-\mu_0 L\right) \right]^{-1/2} \,. \tag{14}$$

in the case of small asymmetries.

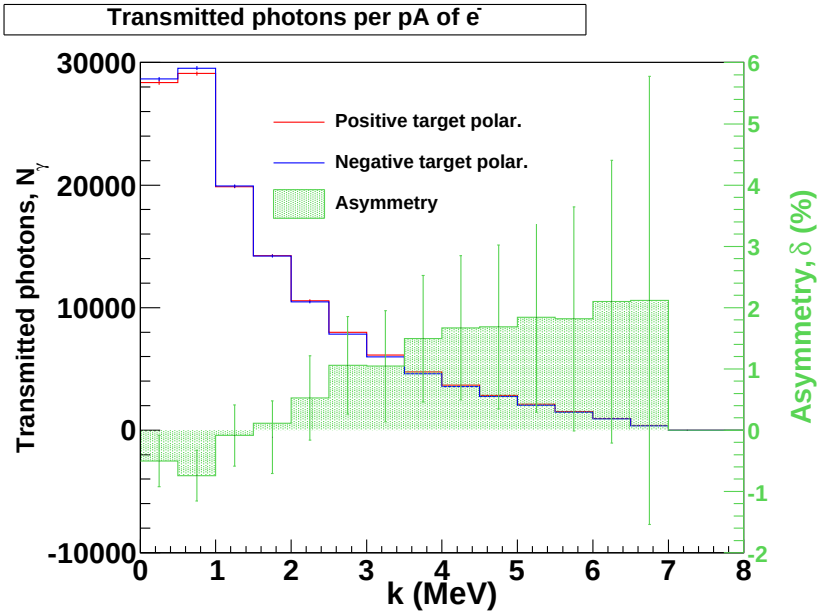

Figure 14. Number of transmitted photons for two opposite target polarization and expected experimental asymmetry as obtained from GEANT4 simulations. The statistical error bars correspond to a data taking time of 1 s at a 1 pA current.

The photon beam of this experiment constitutes of the bremsstrahlung spectrum of mono-energetic polarized electrons or positrons which energy distribution favors small photon energies while the circular polarization distribution favors high photon energies. The resulting experimental asymmetry is then a convolution of this spectrum with the polarized Compton absorption process. This multistep process has been simulated with GEANT4 [17] taking advantage of its upgrade for polarized electron, positron and photon interactions [18]. A 7.5 MeV gaussian electron beam of 400 μm width is converting into photons within a 1 mm thick tungsten target located at 12 mm of a polarized target made-out of an iron cylinder 75 mm in length and 50 mm in diameter. The photon detector is symbolized by a 60×60 mm^2 ideal surface

detection located 72.5 mm from the exit of the polarized target. This geometrical arrangement actually corresponds to the E166 experiment [44]. Fig. 14 shows the number of transmitted photons and the expected asymmetry for 1 pA of electrons and 85 % longitudinal polarization. For each photon energy bin, the electron beam polarization can be inferred from

$$P_e = \frac{A_T}{P_t A_e} \tag{15}$$

where A_e is the electron analyzing power, determined either from simulation or experiment with a known polarized beam. The statistical average over the accepted photon energy range yields the average analyzing power $\overline{A_e} =$ The statistical uncertainty on P_e for a 1 s data taking time at 1 pA is $\delta P_e =$ meaning that an accurate measurement could be obtain within a short amount of time, provided that the detection system is able to handle a MHz event rate. Clearly, the main limitation of the satistical performance of the experiment would originate from the data acquisition rate and not the basic properties of the polarimeter.

4.2 Data acquisition

In order to achieve the statistical accuracy in a reasonable time, a fast acquisition will be designed for the readout of the CsI calorimeter. By using an aggressive pipelining and buffering of the data with the use of flash ADC one could reach easily rates of several hundreds of kilohertz of trigger rates. The proposed system is similar the current Hall A Compton polarimeter, which allowed to record up to 100KHz of trigger in 1999 [**?**]

4.3 Presentation of the device

We borrowed the Transmisson Compton Polarimeter hardware of the experiment E166 [44]. It consists of a conversion target to convert the polarized positron into polarized photons mostly. Those photons are sent through an iron target which is polarized by a magnet. The photons are detected in a Cesium Iodide calorimeter. The photon detector is constituted of 9 Cesium Iodide CsI blocks of 6 cm x 6 cm x 30 cm. Those blocks were fitted with Hamamatsu PMTs. Looking that the photon asymmetry from this detector, one can determine the initial positron polarization.

4.4 Data acquisition system

The data acquisition system is based on the JLAB Flash ADC. This is a VME64X board with a sampling rate of 250 MHz. Having access to all the samples allows to access the polarization using different methods which could give a better control of the systematical error. The most straightforward way

to measure the Compton Asymmetry is to use an integrated approach. The electron beam helicity is flipped at 960 Hz, the method consists in integrating the signal during an helicity window. The results is the asymmetry integrated over the full range of energies of the detected photons. Since the amplitude information is available a semi integrated method will be implemented on the VME CPU, where an histogram will be filled with the pulse energies for pulses over a certain threshold. The histograms are transferred and reset for each helicity period.

4.5 Calibration

Initial energy calibration of the calorimeter will be done using several gamma source such as Cs137, Na22 and Co60 and with cosmics. The final calibration of the device will be done using electrons. Since it is possible to direct the electron beam to the Mott polarimeter or the Compton Transmission polarimeter, the incident beam polarization will be know at least at the 3 % level. This will allow to tune the beam through the different elements of the experiment at higher current where the beam diagnostics are fully working and to determine the response fonction of the detector to accurately extract the polarization.

4.6 Background

Unpolarized background, will be eliminated in the asymmetry but will still dilute the signal. In order to reduce the polarized background which could generate a parasitic asymmetry. Large amounts of shielding will be placed around the detector. Its placement will be optimized using the Geant4 simulation. Data with converter foil out allows to determine the background induce by the primary electron beam. Data with analyzer magnetic field off in the spectrometer dipoles will measure the polarized background not coming from the reconversion foil of the polarimeter.

4.7 Statistical uncertainties

By the nature of the process the efficiency of the device is quite low. Only part of the electron or positron convert into photons in the converter foil and only part of the photons will interact via Compton effect ending with Compton photons in the Cesium Iodide calorimeter

4.7.1 Integrated measure systematic uncertainties

Assuming the usual 85 The expected asymmetry is of the order of 1%. The pedestal width of the electronics is . So a measurement at 0.1% level, given the measured noise σ the measurement should be reached in

4.7.2 Semi-Integrated measure systematic uncertainties

The estimated positron current produced reaching the conversion target will be 1 pA for 1 uA of incident electron beam. From the Geant4 simulation of the Compton polarimeter for 5 MeV incident positron about 2.5e-5 efficiency of photons are collected in the central crystal for the highest energy bin. So 1Total detector rate of photon in the detector is evaluated to be around 80 KHz for 1 pA so dead time will not be an issue even for the semi-integrated method.

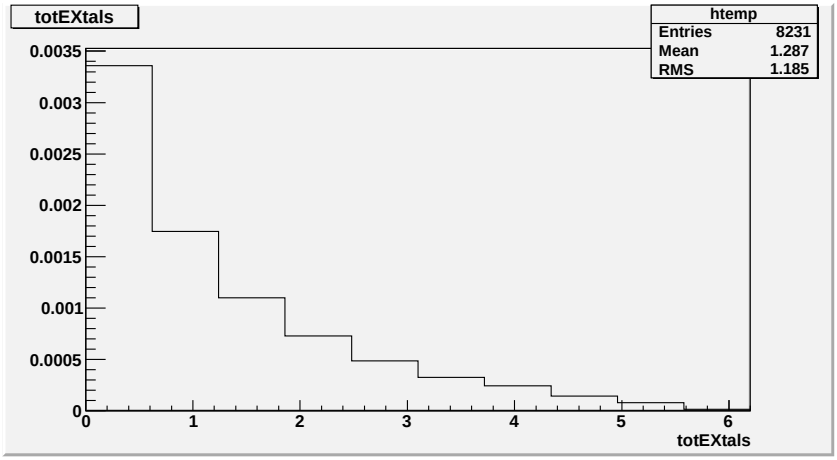

Figure 15. Number of transmitted photons for 10 energy bins and 1 million incident positrons

4.8 Polarization extraction

4.8.1 Charge asymmetry

Since we are measuring a beam asymmetry between two helicity, the charge asymmetry. In order to reduce the correction from the charge asymmetry a charge feedback acting on the source is used. Typically a charge asymmetry feedback can keep the charge asymmetry to less than 100 ppm.

4.8.2 Electronic pick-up

In a first step we will mostly run in time helicity since it makes analysis easy but makes the data potentially sensitive to pick off of helicity correlated electronic noise. In order to alleviate this problem we will still have the possibilty to run with delayed helicity. This method is common for parity experiments measure very small asymmetries. The helicity follows

4.9 Systematical uncertainties

In order to reduce the systematic, analysis will be based on pair analysis similar to the previously ran parity experiments. The fast helicity flip should allow to elimininate all false asymmetries due to slow drift such has magnets field or position changes and calibration variations.

4.9.1 Integrated measure systematic uncertainties

The integrated measurement major advantage is insensitivity to energy calibration and is free of dead time. Though the method has two systematic on the extraction of the polarization :

- the detector non-linearities
- contribution of polarized background.
- dilution by background

Detector linearity will be checked using a pulser and folded in the simulation to extract the polarization. Contribution of background can be determined with the runs with analyzer field on, off and flipped.

4.9.2 Semi-integrated E166 systematic uncertainties

An semi-integrated method is interesting to be studied since the asymmetry grows with energy. Nevertheless this method is very sensitive to the energy calibration of the detector, since the shape of the asymmetry as a function of the energy is fitted to extract the polarization. The systematic uncertainty of this method are :

- PMT gain change as a function of time
- energy response of the detector
- pile up
- position in the detector which can induce leakage.

The relative gain will be monitored by a LED system and regularly checked with radioactive sources to provide an absolute calibration, Contribution of the pile up will be determined with data taking at different currents and running the DAQ in sampling mode to record the full waveforms to study the contribution of the pile up. Response function of the detector will be modeled by the simulation. The data can be cross checked at a photon source such as TUNL in Duke in needed. Collimated runs and looking at the behavior of the asymmetry when more than one block is hit will be taken to assess the effect of leakage to the neighboring blocks.

5 Beam time request

5.1 Commissioning

5.2 Electron calibration

5.3 Positron measurements

5.4 Beam requirements

We request approval for 168 hours of beam time to measure the polarization of positrons produced in the JLab injector. The commissioning of the new beam line and the Compton transmission polarimeter is estimated to take 112 hours of beam time with the remaining 56 hours devoted to beam polarization measurements. Emittance measurements will consume about 24 hours of commissioning time. The commissioning of new beam line monitors and establishing the beam transport to the Compton transmission polarimeter with consume the remaining 88 hours of commissioning time.

Running Condition Number	Beam Energy (MeV)	Beam Current (μA)	Beam Polarization (%)	Target Material	Target Thickness (mg/cm^2)	Beam Time (h)
1	6.2	1-5	> 80	Mott Targ.		4
2	6.2	1-10	> 80	W Con. #1	192.5	16
				W Con. #2	1925	
				W Con. #3	3850	
				Pol. Conv. #1	1925	
				Pol. Conv. #2	3369	
				Pol. Targ.		
3	6.2	1-10	> 80	Ann. Targ.		24
				Fiber Detector		

Table 2

Beam polarization measurements will be made with the Mott and Compton transmission polarimeters over a 56 hours period. The first measurement will compare the polarization of 6.2 MeV electron beam measured using the Mott polarimeter to the polarization measured in the Compton transmission polarimeter. A Tungsten converter target will be inserted to produce positrons. We plan to repeat the electron polarization measurement with the Tungsten target inserted using the Compton transmission polarimeter for comparison and then proceed with a positron measurement. The table below identifies the

beam time for the physics measurements performed by this experiment.

References

[1] P.W. Higgs, *Phys. Rev. Lett.* **13** (1964) 508.

[2] F.E. Maas *et al.*, *Phys. Rev. Lett.* **94** (2005) 152001.

[3] D.S. Armstrong *et al.*, *Phys. Rev. Lett.* **95** (2005) 092001.

[4] K.A. Aniol *et al.*, *Phys. Rev. Lett.* **96** (2006) 022003.

[5] R.D. Young, R.D. Carlini, A.W. Thomas, J. Roche, *Phys. Rev. Lett.* **99** (2007) 122003.

[6] Proceedings of the International Workshop on Positron at Jefferson Lab, Edts. L. Elouadrhiri, T.A. Forest, J. Grames, W. Melnitchouk, and E. Voutier, *AIP Conf. Proc.* **1160** (2009).

[7] H.A. Olsen, L.C. Maximon, *Phys. Rev.* **114** (1959) 887.

[8] T. Omori *et al*, Phys. Rev. Lett. **96** (2006) 114801.

[9] G. Alexander *et al*, Phys. Rev. Lett. **100** (2008) 210801.

[10] J. Dumas, J. Grames, E. Voutier, *AIP Conf. Proc.* **1149** (2009) 1184.

[11] W.H. McMaster, *Rev. Mod. Phys* **33** (1961) 8.

[12] B.A. Mecking *et al.*, *Nucl. Inst. Meth.* **A 503** (2003) 513.

[13] E.G. Bessonov, A.A. Mikhailichenko, *Proc. of the V^{th} European Particle Accelerator Conference*, Barcelona (Spain), June 10-14, 1996.

[14] A.P. Potylitsin, *Nucl. Inst. Meth.* **A 398** (1997) 395.

[15] J. Grames *et al.*, *Proc. of the 2007 Particle Accelerator Conference*, Albuquerque (New Mexico, USA), June 25-29, 2007.

[16] J. Dumas, J. Grames, E. Voutier, *AIP Conf. Proc.* **1160** (2009) 120.

[17] S. Agostinelli *et al*, Nucl. Inst. Meth. **A 506** (2003) 250.

[18] R. Dollan, K. Laihem, A. Schälicke, Nucl. Inst. Meth. **A 559** (2006) 185S.

[19] E.A. Kuraev, Y.M. Bystritskiy, M. Shatnev, E. Tomasi-Gustafsson, *Phys. Rev. C* **81** (2010) 055208.

[20] D. Müller, D. Robaschick, B. Geyer, F.M. Dittes, J. Hořejši, *Fortschr. Phys.* **42** (1994) 101.

[21] A.V. Radyushkin, *Phys. Rev.* **D 56** (1997) 5524.

[22] M. Diehl, *Phys. Rep.* **388** (2003) 41.

[23] M. Burkardt, *Phys. Rev.* **D 62** (2000) 071503.

[24] J.P. Ralston, B. Pire, *Phys. Rev.* **D 66** (2002) 111501.

[25] M. Diehl, *Eur. Phys. Jour.* **C 25** (2002) 223.

[26] A.V. Belitsky, D. Müller, *Nucl. Phys.* **A 711** (2002) 118c.

[27] A.V. Belitsky, A.V. Radyushkin, *Phys. Rep.* **418** (2005) 1.

[28] X. Ji, *Phys. Rev. Lett.* **78** (1997) 610.

[29] M. Burkardt, *Phys. Rev.* **D 72** (2005) 094020.

[30] X. Ji, J. Osborne, *Phys. Rev.* **D 58** (1998) 094018.

[31] J.C. Collins, A. Freund, *Phys. Rev.* **D 59** (1999) 074009.

[32] A. Airapetian *et al.*, *Phys. Rev. Lett.* **87** (2001) 182001.

[33] S. Stepanyan *et al.*, *Phys. Rev. Lett.* **87** (2001) 182002.

[34] C. Muñoz Camacho, A. Camsonne, M. Mazouz, C. Ferdi, G. Gavalian, E. Kuchina *et al.*, *Phys. Rev. Lett.* **97** (2006) 262002.

[35] M. Mazouz, A. Camsonne, C. Muñoz Camacho, C. Ferdi, G. Gavalian, E. Kuchina *et al.*, *Phys. Rev. Lett.* **99** (2007) 242501.

[36] F.-X. Girod, R.A. Niyazov *et al.*, *Phys. Rev. Lett.* **100** (2008) 162002.

[37] M. Diehl, *CLAS12 European Workshop*, Genova (Italy), February 25-28, 2009; *http://www.ge.infn.it/∼clas12/talks/thursday_session6/diehl-genova.pdf*

[38] M. Guidal, *Eur. Phys. J.* **A 37** (2008) 319.

[39] H. Moutarde, *Phys. Rev.* **D 74** (2009) 094021.

[40] P.-Y. Bertin, C.E. Hyde, C. Muñoz Camacho, J. Roche *et al.*, *Jefferson Lab Prop.* **PR-07-007** 2007.

[41] R. Krause-Rehberg, H.S. Leipner, *Positron Annihilation in Semiconductors*, ISBN 3-540-64371-0 Springer-Verlag Berlin Heidelberg New York, 1999.

[42] S. Tanigawa, A. Uedono, L. Wei, R. Suzuki, *Positron Spectroscopy of Solids*, A. Dupasquier, J. Mills eds., IOS Press Amsterdam, 1995, 729.

[43] V. Angelov, E. Voutier, *work in progress.*

[44] G. Alexander *et al*, Nucl. Inst. Meth. **A 610** (2009) 451.